ChemCatChem

Research Article
doi.org/10.1002/cctc.202301578

Chemistry Europe
European Chemical Societies Publishing

www.chemcatchem.org

Measurement of Enthalpy and Entropy of a Model Electrocatalyst for the Oxygen Evolution Reaction

Joaquín Morales-Santelices[a] and Marcel Risch*[a]

Experimentally determined thermodynamic parameters are rarely reported for electrocatalytic reactions including the oxygen evolution reaction (OER). Yet, they contain unique and valuable mechanistic insight and present a missing link to theoretical investigations. Herein, a protocol for determining thermodynamic properties of the rate determining state and intermediate (RDSI) of the OER is presented. Cobalt oxide is investigated at pH 7 as a case study. Two different approaches are employed: steady state polarization (SSP) that uses chronopotentiometry at different temperatures and current values, and potentiostatic electrochemical impedance spectroscopy (PEIS) at different DC voltages and temperatures. The data is used to fit a 3D plane from which entropy and enthalpy of the RDSI are obtained. The data analysis requires an appropriate filtering of the data. Hence, we discuss suitable figures of merit for establishing appropriate filtering criteria. The values obtained are 0.72 and −0.39 eV (at 298 K) for enthalpic and entropic contributions, respectively. The obtained values are reproducible for both approaches and consistent with literature.

Introduction

To increase the amount of hydrogen production using green sources of energy, water electrolyzers should use more durable, cheap, and active electrocatalytic materials for the water splitting reaction (WSR).[1–5] For these purposes, it is vital to understand the mechanisms of the hydrogen and oxygen evolution reactions (HER and OER) on the surface of the electrocatalysts in a thorough way. These paths explain how to decrease the high energy of activation,[6] how to improve measures of the specific activity such as the turnover frequency (TOF), and/or how to maximize the faradaic efficiency. Of the two half-reactions, the OER is the more sluggish one, and therefore, the one that needs further optimization.[7]

For more than a century, the Sabatier principle[8] has been used as a guideline in heterogeneous catalysis, where it is desirable to have catalysts with binding energies (and/or other types of performance descriptors) inside a certain range that ensures that the bond is neither too strong nor too weak. In electrocatalysis of the OER, this analysis is frequently done by calculating relevant thermodynamic properties and the resulting theoretical overpotential[9–10] or identifying experimental correlations.[11] Tweaking the binding energies by modifying either the catalyst composition or the OER conditions, allows us to engineer the steps undergone and encourage certain pathways while discouraging others.

Transition State Theory (TST)[12] relates relative energies between intermediates and transition states (TS) of elementary steps to the overall reaction rate (concept of energetic span coined by Amatore and Jutand[13] and discussed by Kozuch and Shaik[14]).

For our analysis we will use the TST, and therefore it will be assumed that: (1) The coverage of active sites is constant in the analyzed region. (2) The steps before TS are in quasi-equilibrium. (3) One active site is clearly predominant. (4) When a system exhibits Tafel behavior, every Tafel region with one slope value is linked to one rate-determining state and intermediate (RDSI).[15] This way, the change in the energetic profile of OER could be depicted as shown in Figure 1a.[16–17]

It is known that the elementary steps of a mechanism contribute to various degrees to the overall reaction rate. When only one state and one intermediate have degree of rate control (DRC)[18] approaching 1 and the others have a neglectable DRC value (close to 0) we will refer to the mentioned state and intermediate as rate-determining.[19] In the literature is has been accepted DRC values higher than 0.75 as an acceptable threshold to assign the RDSI.[20]

To describe the RDSI of an electrocatalytic reaction, the following parameters are needed: enthalpy ($\Delta^{\ddagger}H$), entropy ($\Delta^{\ddagger}S$), Gibbs free energy ($\Delta^{\ddagger}G$) and transfer coefficient (β). These thermodynamic parameters have been previously investigated theoretically[21–23] and experimentally.[17,24–27] All equations used for the description of these key parameters are explained in Section S1 of SI.

Continuing with the idea of the search for cheaper, more abundant, but also more efficient and durable OER catalysts, first row transition metal oxides such as Fe, Mn, Co, Ni have outstanding electrocatalytic characteristics in neutral and alkaline media and are earth-abundant.[28–30] In the case of cobalt, there is one catalyst, amorphous cobalt oxide with molecular

[a] J. Morales-Santelices, Dr. M. Risch
Nachwuchsgruppe Gestaltung des Sauerstoffentwicklungsmechanismus
Helmholtz-Zentrum Berlin für Materialien und Energie GmbH
Hahn-Meitner Platz 1, 14109, Berlin, Germany
E-mail: marcel.risch@helmholtz-berlin.de

Supporting information for this article is available on the WWW under https://doi.org/10.1002/cctc.202301578

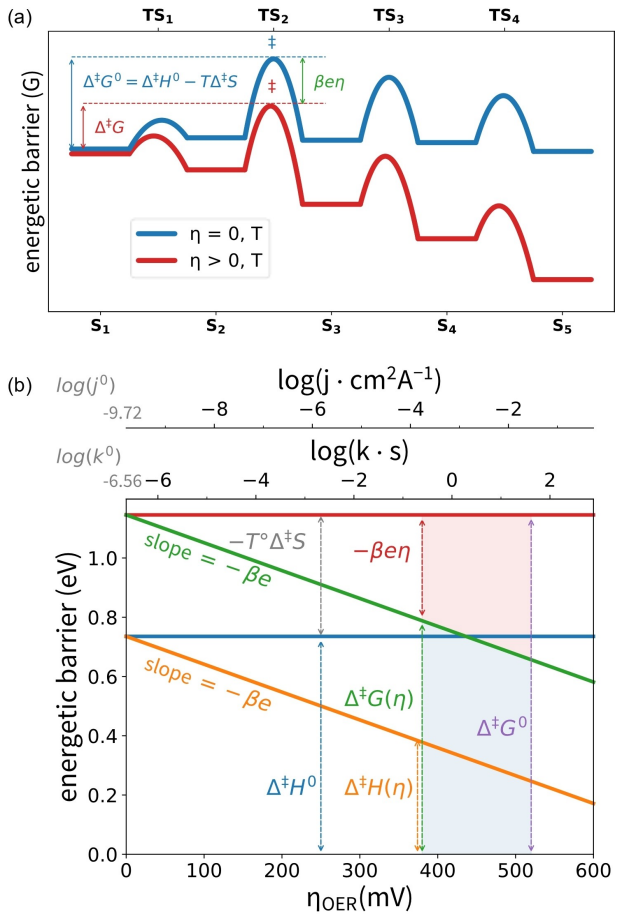

Figure 1. Conceptual background. (a) Gibbs free energy profile of the OER happening on an electrocatalyst's surface. The energy levels of the different states and intermediates are shifted when changes in overpotential or temperature occur. For the construction of this particular diagram it has been assumed that S_1 and TS_2 are the rate determining state and intermediate, respectively (RDSI). The apparent transfer coefficient β will be in this case equal to $1 + \alpha_2$ (transfer coefficient of elementary step from S_2 to S_3 using the Butler-Volmer formalism[16]) (Note that the labeling of the states is arbitrary and irrelevant in this formalism). (b) Interrelation between the thermodynamic parameters of the OER RDSI for CoCat obtained using the values reported in the work of Lee and coworkers[17] evaluated at 25 °C. The energetic barrier has different contributions (enthalpic, entropic and overpotential) and is related to the kinetic constants and current densities as stated by Equations S1 to S9. The shaded zone shows the zone where the Tafel behavior was observed. These values were extrapolated to zero overpotential to give more clarity conceptually.

properties (CoP_i, referred to as CoCat herein), discovered by Kanan and Nocera in 2008,[31–33] that has been widely studied since then.[34] This is because: it is easy to synthesize (via electrodeposition), it can drive OER in neutral media, giving better safer operating conditions, is more compatible with natural waters. Additionally, it shows self-healing.[33,35]

The thermodynamic parameters of the OER for oxides containing Co can be found in the literature (see Figure 1b), mostly coming from theoretical works, including a diagram of Gibbs free energy (G) at the elementary steps of each of the four electron transfers (energy of five states in total, restricted by OER thermodynamics and scaling relations).[9,36–39] Few reports discuss the intermediates between steps and calculate their respective energies, which would better connect to kinetic experimental work.

Theoretical investigations rely mostly on density functional theory (DFT), and sometimes combine it with molecular dynamics (MD)[23] or microkinetic simulations.[40,41] In these works, a mechanism for OER on the surface of the Co-based oxide is suggested. A Gibbs free energy profile (or E-representation)[14,42] is calculated at given conditions where a certain surface coverage is expected (according to surface Pourbaix diagrams of Co oxides).[22] From these energy profiles, the potential-determining step (PDS) can be elucidated (Figure 1a).[43] In some works, kinetic information such as the RDSI enthalpy was obtained from the enthalpy associated to the energetic span.[21,22]

In experimental investigations, the value of the RDSI enthalpy is determined (even when the mechanism is not known) using either Arrhenius[24,25] or Eyring-Polanyi[17] plots where the former is more frequently used but the latter is a more straightforward treatment. These plots can be built from different types of temperature dependent experiments: linear sweep or cyclic voltammetry (LSV or CV),[17] techniques such as chronoamperometry (CA) or chronopotentiometry (CP)[24–26] or electrochemical impedance spectroscopy (EIS).[30] It is important to note, that to have a reliable result, one needs to ensure that: (1) the current measured corresponds to OER rather than other reactions or to non-faradaic current.[44] (2) the kinetics is limited by charge-transfer at these range of overpotential[45] (3) the system achieves steady state polarization condition (SSPC): the current and potential reach a stable value under a sufficiently large certain period of time (defined by a drift criterion)..[46–47]

For the reasons mentioned, it is strongly recommended to prefer potentiostatic/galvanostatic instead of voltametric techniques and leave the applied potential for long time enough to ensure that is has arrived effectively to SSPC. Key thermodynamic parameters for selected Co oxides are compiled in Table 1[17,24,26,27,36,48] for experimental studies.

In this work, we provide a protocol to experimentally determine the key thermodynamic parameters $\Delta^{\ddagger}H^0$, $\Delta^{\ddagger}S$, $\Delta^{\ddagger}G$ and β for the OER on CoCat as a case study. CoCat is used since it is an easy-to-prepare and widely studied material. The electrolyte is 0.1 M phosphate buffer at pH 7. We propose a combined synergistic approach between CP and potentiostatic EIS (PEIS) to tackle their individual disadvantages. Finally, we compare the accuracy of both methods and discuss the results in the context of the present literature on this electrocatalyst.

Experimental Setup

Details of the electrochemical system are given in Section S2 A graphical description of the setup is shown in Section S3 (Scheme S1). The working electrode (WE) consists of bare fluorine-doped tin oxide (FTO)-coated glass sonicated in a concentrated nitric acid solution in water (13 % HNO_3) for 10 minutes and rinsed with DI water. The platinum wire used as counter electrode (CE) was cleaned with the same procedure.

All potentials that are reported in V vs reference electrode (RE) refer to a saturated Ag | AgCl | KCl electrode at a mentioned temperature

Table 1. Enthalpies of the RDSI for OER driven in Co-oxide-containing materials found in experimental studies in the literature.

Material	Parameter	Value	Conditions	Method	Ref.
CoCat	$\Delta^{\ddagger}H$	0.74 eV	**@ $\eta = 0.410$ V** (@1 mA cm^{-2}) 20 mV s^{-1} pH = 7.0 $p_{O2} = 0.21$ atm KPi 0.1 M 20 to 70 °C	Multi T LSV	[17]
	$\Delta^{\ddagger}G$	0.74 eV 0.75 eV	**@ $\eta = 0.410$ V** KPi 0.1 M pH = 7.0 **@ $\eta = 0.410$ V** KPi 0.1 M pH = 7.0	 SI-SECM SI-SECM	[27] [48]
LDH FeCo G-FeCo G-FeCoW A-FeCoW	$\Delta^{\ddagger}H$	0.84 eV 0.62 eV 0.51 eV 0.83 eV	**@ $\eta = 0.300$ V** Au(111) substrate 1 M KOH 294 to 357 20 to 80 °C	Multi T CA	[36] [36] [36] [36]
NiCoP NiCoFeP IrO_2	$\Delta^{\ddagger}H$	0.39 eV 0.28 eV 0.31 eV	**@ $\eta = 0.700$ V** Au(111) substrate CO_2-saturated 0.5 M $KHCO_3$ 18 to 35 °C	Multi T LSV	[26] [26] [26]
$NiCo_2O_4$	$\Delta^{\ddagger}H^0$	0.72 eV	**@ $\eta = 0$** 1 mV s^{-1} 30% w/w KOH 0° to 160 °C	Multi T CA	[24]

unless the contrary is stated. All overpotentials are reported in mV and a distinction is made between overpotential before and after iR_u correction (η' and η, respectively).

CoCat films were prepared right before the temperature-dependent Tafel analysis. The electrodeposition precursor (namely Electrolyte 1) was a solution of phosphate buffer 0.1 M pH = 7.0 (KH_2PO_4 *Sigma Aldrich*, 99.5% purity; $K_2HPO_4 \cdot 3\ H_2O$ *Honeywell*, 99.5% purity) and 0.5 mM Co^{II} ($Co^{II}(OH_2)_6(NO_3)_2$ *Sigma Aldrich*, 99.9% purity). The electrolytes were left inside the climate chamber to equilibrate with the atmospheric pressure at a controlled temperature of 25 °C to reach air saturation. The film synthesis consisted in a chronopotentiometry with a two-electrode configuration using a current of 12 μA cm^{-2} for 750 s, when a total charge of 9.0 mC have passed (WE area is 0.90 cm^2, therefore the charge density is 10 mC cm^{-2}).

As soon as the film was deposited, the WE with the catalyst and the CE are removed from the solution. The CE was rinsed with DI water and then dried, Electrolyte 1 rests were wiped from the WE and then both were transferred to a solution without Co^{II} containing phosphate buffer 0.1 M adjusted to pH 7.0 (namely Electrolyte 2) to be conditioned using a three-electrode configuration with a RE. This process consisted of 100 voltammetric cycles starting from 0.9 V having 1.15 V and 0.40 V (all vs RE) as higher and lower limit, respectively. This treatment was sufficient to ensure that the shape of the CV did not change further. Except from the short lapse where the material was changed from Electrolyte 1 to Electrolyte 2, a fixed potential value was always applied on the WE to avoid degradation. The CV scan rate was 100 mV s^{-1}.

Results and Discussion

In general, experimental calculation of the enthalpy of the RDSI requires temperature-dependent experiments, during which the geometric and electronic structure should not change. Our protocol has an experimental part and a data treatment part as summarized in Scheme 1 and Scheme 2, respectively.

Experimental protocol

As seen in Scheme 1a, the protocol has three measurement steps: (1) equilibration (EQ), (2) CP and PEIS measurements for construction of multi-temperature Tafel plots and fitting Eyring-Polanyi equation and (3) CV to determine the redox activity. The length of the equilibrating procedures was such that could ensure that the experimental setup has reached thermal equilibrium at the beginning of each step (see details in Section 2B Figure S1). Parameters, and raw data are accessible at Zenodo.[49]

After 3 h of thermal equilibration between the climate chamber and the beaker, the temperature registered with the thermocouple inside the electrolyte stabilizes and do not fluctuate during the rest of the iteration. Due to the latter, it was assumed that thermal equilibrium between the beaker and the air in the chamber was reached (more details in Section S4

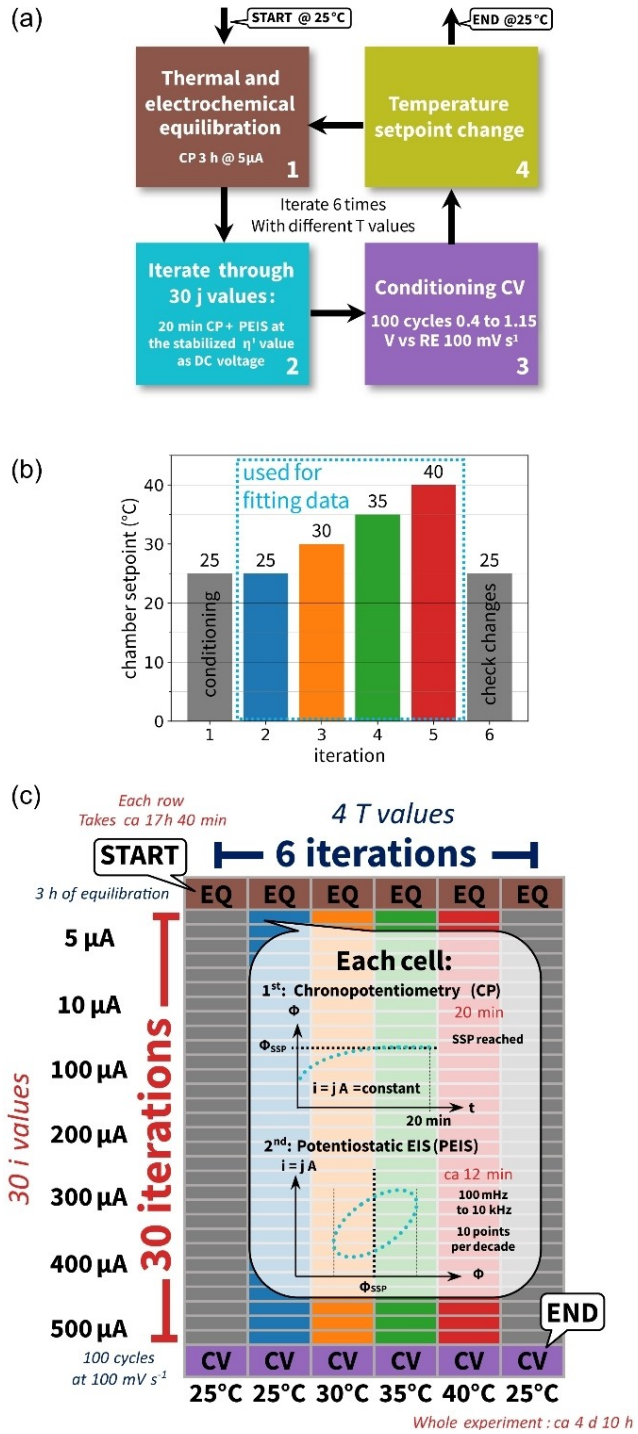

Scheme 1. Experimental protocol. (a) Flowchart containing the protocol used for this work. (b) Temperature steps program used in the climate chamber for these measurements. The iterative loop was repeated 6 times herein. The first and last iteration are used for conditioning and tracking irreversible changes, respectively. (c) Diagrammatic representation of the followed protocol for scanning the studied j × T region and discard the presence of irreversible changes in the material.

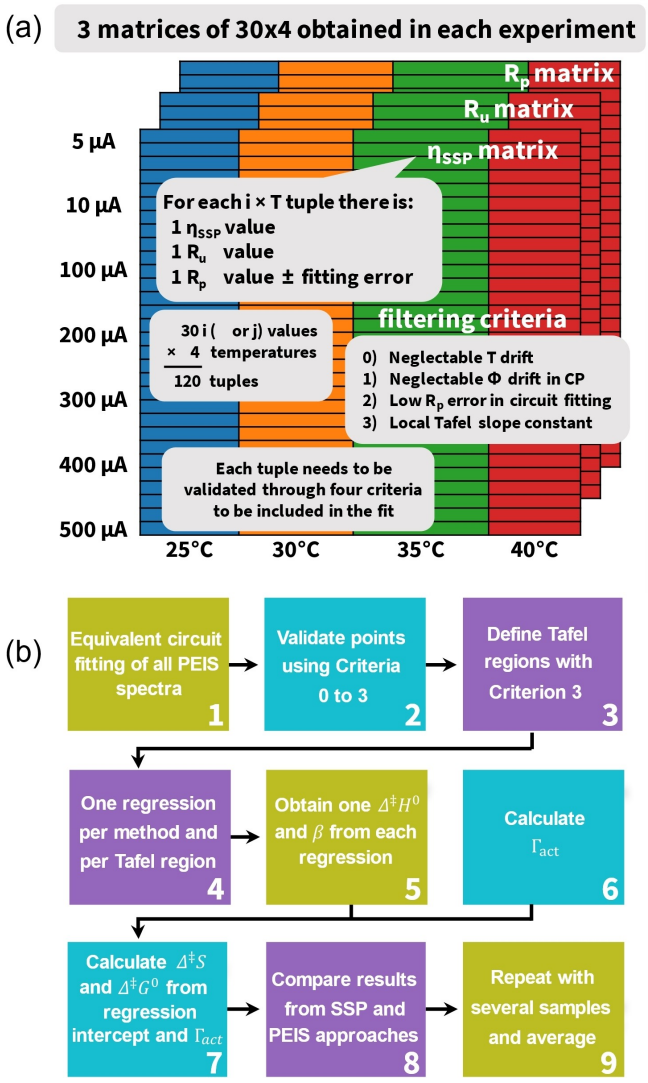

Scheme 2. Protocol for data analysis. (a) The experimental data obtained from the experiments explained in Scheme 1 are summarized in 3 matrices. (b) Steps followed to analyze data and obtain the thermodynamic values in this work. Details are discussed in the main text and in Section S5. Criteria are described in Table 3.

Figure S2). We investigated temperatures between 25 °C and 40 °C in 5 °C steps. Temperatures higher than 40 °C were not used because the increase in the evaporation rate of the solvent during the long experiment resulted in a sizable change in the electrolyte volume and consequently exposed area of the sample in our current setup.

Data treatment protocol

Once the full set of experiments is performed and iR_u compensated (details in Section S6 Scheme S2 and Figure S5), the SSP value of current density can be obtained as the arithmetic mean of the 10 last chronoamperometric points measured (to decrease noise). Only the η×T tuples that fulfill a SSPC are used in the next step. We used a maximum tolerance value permitted in the overpotential drift: within the last 10 minutes of every CP, the overpotential must not change more than ±0.65 mV. We will refer to this as Criterion 1. Additional details are found in Section S5.

To construct the Eyring-Polanyi plane, Equations S5, S7, S8 and S9 were combined, divided by T and the natural logarithm was taken. This results in a 3D plane version convenient for OER, under the assumption that $\Delta^{\ddagger}H^{\circ}$, $\Delta^{\ddagger}S$ and Γ_{act} are invariant within temperature and current/overpotential regions (where there is one type of coverage being predominant):

$$\frac{\eta}{T} = \frac{\Delta^{\ddagger}H^{0}}{\beta e}\left(\frac{1}{T}\right) + \frac{k_B}{\beta e}\ln\left(\frac{j}{T}\right) - \frac{\Delta^{\ddagger}S}{\beta e} - \frac{k_B}{\beta e}\ln\left(z_e e\kappa\frac{k_B}{h}\Gamma_{act}\right) \quad (1a)$$

Or writing (1a) as a plane equation in 3 dimensions:

$$z = C_1 x + C_2 y + C_3 \quad (1b)$$

With variables:

$$x = \frac{1}{T} \quad (1c)$$

$$y = \ln\left(\frac{j}{T}\right) \quad (1d)$$

$$z = \frac{\eta}{T} \quad (1e)$$

And coefficients:

$$C_1 = \frac{\Delta^{\ddagger}H^{0}}{\beta e} \quad (1f)$$

$$C_2 = \frac{k_B}{\beta e} \quad (1g)$$

$$C_3 = -\frac{\Delta^{\ddagger}S}{\beta e} - \frac{k_B}{\beta e}\ln\left(z_e e\kappa\frac{k_B}{h}\Gamma_{act}\right) \quad (1h)$$

This will be called the SSP approach.

Analogous to what is discussed in the work of Doyle, Godwin, Brandon and Lyons,[30] a partial derivative respect to η can be applied to Equation 1a. Knowing that, within the charge transfer limiting region, the faradaic resistance (per unit of area) is given by:

$$\frac{\partial j}{\partial \eta} = \frac{1}{R_f A} = \frac{1}{\tilde{R}_f} \quad (2)$$

An alternative linearized Eyring-Polanyi equation can be generated by obtaining the partial derivative respect of η in Equation (1a) and rearranging terms:

$$\ln\left(\frac{1}{\tilde{R}_f}\right) = \frac{-\Delta^{\ddagger}H^{0}}{k_B}\left(\frac{1}{T}\right) + \frac{\beta e}{k_B}\left(\frac{\eta}{T}\right) + \frac{\Delta^{\ddagger}S}{k_B} + \ln\left(\frac{z_e\beta e^2\kappa\Gamma_{act}}{h}\right) \quad (3a)$$

The new 3D plane equation is:

$$z' = C_1' x' + C_2' y' + C_3' \quad (3b)$$

with variables:

$$x' = \frac{1}{T} \quad (3c)$$

$$y' = \ln\left(\frac{j}{T}\right) \quad (3d)$$

$$z' = \frac{\eta}{T} \quad (3e)$$

and coefficients:

$$C_1' = \frac{-\Delta^{\ddagger}H^{0}}{k_B} \quad (3f)$$

$$C_2' = \frac{\beta e}{k_B} \quad (3g)$$

$$C_3' = \frac{\Delta^{\ddagger}S}{k_B} + \ln\left(\frac{z_e\beta e^2\kappa\Gamma_{act}}{h}\right) \quad (3h)$$

This will be called the PEIS approach where $\tilde{R}_f$ is obtained by fitting an equivalent circuit (Scheme S2) to the EIS spectrum obtained at DC overpotential η using *Gamry Analyst 2.0*. Further details of this approach are found in Section S6. Polarization resistance results (Figure S5) obtained by equivalent circuit fitting are also filtered according to Criterion 2: Discard any data where SSPC was not fulfilled or points where the regression error calculated for the polarization resistance is greater than 50% of the R_2 value. Finally, the coefficients in Eq. (1) and (3) were obtained with a bilinear regression fitting of the respective experimental dataset using the Python library module *SciPy* (submodule *stats*).

Results

The experimental procedure was repeated three times in two identical electrochemical environments that were running simultaneously inside the climate chamber, generating in total 6 independent sets of data.

Figure 2 shows the general trend obtained at a fixed temperature with increasing DC potential at lower frequency range (100 mHz to 5 Hz). To see examples of the complete frequency range spectra refer to Section S6 (Figure S3).

In Figure 3, two approaches for Tafel plots are compared: (1) SSP and (2) PEIS. Even though the lines obtained from SSP appear straight by eye, the instantaneous Tafel slope (discrete derivative, analog to a previous work of our group[50] between consecutive points increases (Figure S7). As one of the assumptions of validity is that coverage and Tafel slope are constant that region, a third criteria is necessary: the instantaneous Tafel slope on that point, that could be approximated as the forward discrete derivatives (see formulas in Section S5) for SSP and PEIS approach, respectively. Criterion 3 for this dataset was defined to consider a zone to

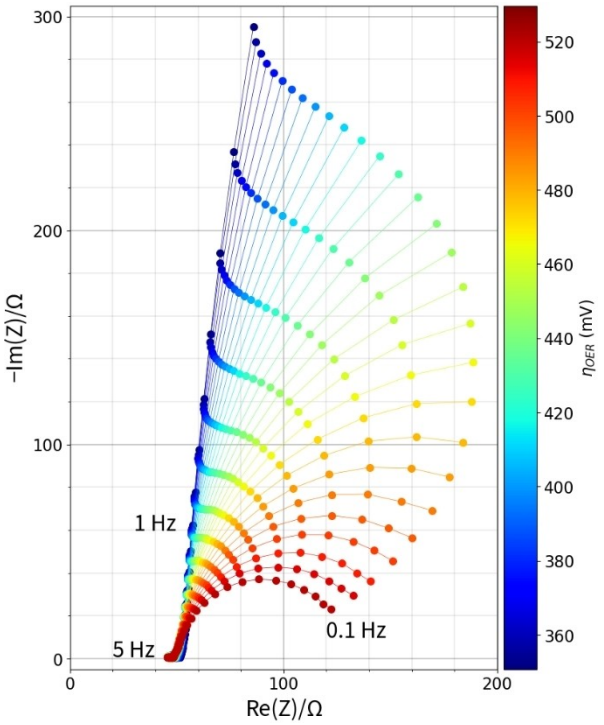

Figure 2. Nyquist plot of part of the PEIS spectra of CoCat electrodes at a temperature of 25 °C at different overpotentials. The values chosen as DC voltage for PEIS are the SSPC values reached during CP. Same trend is observed for subsequent iterations at different temperatures. Continuous line connects points obtained at the same DC potential (and therefore same η_{OER}) between frequency values of 0.1 Hz (rightmost points) and 5 Hz (downmost points), 10 points per decade and 10 mV AC voltage rms. Complete PEIS (from 100 mHz to 100 kHz) is shown in Section S6 (Figure S3). Dataset 2349 A is shown in this plot. The results of fitting all the datasets to equivalent circuits can be seen in Section S6 (Figure S5).

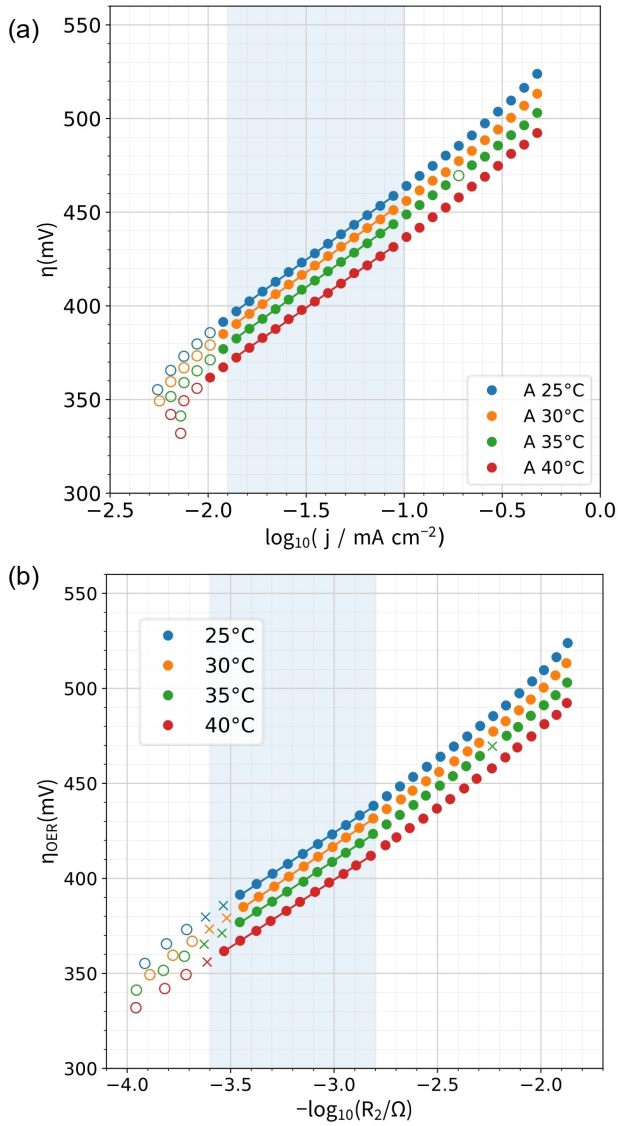

Figure 3. Tafel plots obtained at different temperatures using the results given by: (a) SSP and (b) EIS approaches. Nomenclature: ● fulfills both Criterion 1 and 2 (potential drift < 0.65 mV and fitting error smaller than 50% of the value, respectively). ○: does not fulfill Criteria 1 (for SSP, for PEIS does not fulfill Criterion 1 or 2). ×: does not fulfill Criterion 1 but fulfills Criterion 2. +: fulfills Criterion 1 but does not fulfill Criterion 2. Points fulfilling Criterion 3 (instant Tafel slope in the range 70 to 80 mV dec^{-1}) have been grouped in the blue-shaded area, which indicate that they have Tafel behavior and will be used for subsequent analysis steps. Points outside the blue area do not fulfill Criteria 3 so are also excluded from the next stage of the analysis (construction of Eyring-Polanyi bilinear plots). Only dataset 2349 A is shown this plot. The results of all datasets are shown in Section S9 (Figures S8 and S9) and it can be seen how Criteria 3 was applied.

have Tafel behavior where b_i is within a range of ±5 mV, namely 70 to 80 mV dec^{-1}, for at least 1 decade. Instantaneous Tafel plots were used exclusively as a diagnostic to decide the span of the Tafel zone for linear regression analysis and are displayed in Section S8 (Figure S7). Using Criteria 1 and 3 for SSP and 1,2 and 3 for PEIS approach, the results are consistent with the expected trend of slightly increasing slope value as it is proportional to the absolute temperature according to Equation 6. The range of current density used is 10 to 100 μA cm^{-2} (η values between 360 to 420 mV for SSP and 340 to 440 for PEIS approach). Because of Criteria 3, no other regions in higher or lower overpotentials were deemed as Tafel regions. 0.1 M KPi was used as a proton buffer in a single compartment; these conditions were chosen to prevent change of the local and bulk pH, respectively.[51]

As each tuple starts with 20 min of CP at a current value obtained with potentials where Co(II) experiences oxidation, most part of the sites are already oxidized when the PEIS starts. That is the reason why the contribution of this faradic process to the total charge transfer resistance is much lower when compared to the OER one using 10 mV rms as AC voltage.

The construction of an Eyring-Polanyi plot in 3D can be used to visually assess the degree of bilinearity of the data, corroborated with the determination of the goodness of fit. From the regression coefficients (either C_1, C_2, C_3 or C_1', C_2', C_3') and the aid of the estimation of the film's reductive charge of $1.5 \cdot 10^{15}\ cm^{-2}$ by Equation S24, two independent set of parameters were determined (one per each approach per Tafel region).

These parameters were generated separately for each repetition of the experiments and statistics were obtained. The result found by the two approaches and different repetitions are presented in Table 2. The Criteria used for filtering data and obtaining these values are also summarized in Table 3.

Discussion

Validity of equations, approximations and precautions

Not all the points obtained by SSP/PEIS approach are usable. The points should: (1) have reached the SSPC by keeping the current density constant for sufficiently long time and reaching a constant (over)potential value, (2) in the case of PEIS approach, have a neglectable fitting error, (3) have neglectable diffusional limitations (4) exhibit Tafel behavior for a sufficiently large range of current (or polarization resistance) (5) be iR_u compensated, (6) not be in a zone where DRC is shared between more than one elementary step, since then the density of active sites, Γ_{act}, is not constant, and (7) be in thermal equilibrium. Extended discussion can be found in Section S10 of SI.

PEIS approach

From the PEIS analysis, two processes with different time constants were noted (Section S6 Figure S3): (1) at high frequencies (between 1 and 10 kHz), corresponding to the part with $Re(Z) < 50\ \Omega$ in Nyquist plot of Figure 2 and (2) at low frequencies (< 10 Hz) corresponding to the greater semi circles at $Re(Z) > 50\ \Omega$. This idea is also supported by distribution of relaxation times (DRT) plots available in Section S6 Figure S4. To keep the simplicity during the EIS fitting process, only the frequencies lower than 5 Hz were used to fit a Randles cell with constant phase element (CPE) (see details in Section S6 Scheme S2). The choice for a CPE rather than a simple capacitor was supported by the dispersion in the DRT plot (Figure S4). The absence of relaxation times higher than the one associated to charge transfer, supports the hypothesis of neglectable diffusional effects and a kinetically controlled electrochemical process. This fact is needed for the validity of Equations 1 and 16. Nevertheless, the values used for the determination of the compensated resistance are values obtained at high frequency (100 kHz) where the phase angles were close to 0. As expected from a faradic process, the polarization resistance decreases with increase of η_{OER}, correlated to the curvature of the lines connecting points.

PEIS measurements in CoCat at DC potentials different than OCP have been reported in the literature.[52] Works such as the one of Neerugatti, Adhikari and coworkers[52] suggest

Table 2. Ranges of Tafel slope between 25 °C and 40 °C, RDSI parameters at zero overpotential obtained by SSP and EIS approaches between 25 and 40 °C, and 6 and 566 mA cm^{-2}.

Parameter	SSP	PEIS
η range (mV)	370 to 430 (25 °C) 390 to 460 (40 °C)	360 to 410 (25 °C) 390 to 440 (40 °C)
j range (μA cm^{-2})	12 to 100 μA cm^{-2}	10 to 100 μA cm^{-2}
b range (mV dec^{-1})	70 to 80	70 to 80
β	0.79 ± 0.02	0.85 ± 0.06
$\Delta^{\ddagger}H^0$ (eV)	0.72 ± 0.05	0.81 ± 0.06
$\Delta^{\ddagger}S^0$ (meV K^{-1})	-1.62 ± 0.14	-1.32 ± 0.19
$T^{\circ}\Delta^{\ddagger}S^0$ (eV)*	-0.48 ± 0.04	-0.39 ± 0.06
$\Delta^{\ddagger}G^0$ (eV)*	1.21 ± 0.02	1.20 ± 0.03
Γ (cm^{-2})	$1.5 \cdot 10^{15}$	$1.5 \cdot 10^{15}$
k^0 (s^{-1})*, **	$(3.07 \pm 2.02) \cdot 10^{-8}$	$(5.6 \pm 5.9) \cdot 10^{-8}$
j^0 (A cm^{-2})*, **	$(9.84 \pm 6.46) \cdot 10^{-11}$	$(3.92 \pm 4.18) \cdot 10^{-11}$

* $T^{\circ}\Delta^{\ddagger}S$, $\Delta^{\ddagger}G^0$, k^0, j^0 values were calculated at $T^{\circ} = 25\,^{\circ}C = 298$ K. ** Note that the large standard deviation is due to a the PEIS analysis of dataset EXP2351B. Without it $k^0_{PEIS} = (2.68 \pm 1.70)\ 10^{-7}\ s^{-1}$.

Table 3. Criteria employed for data filtering in this work and the values used to obtain parameters shown in Table 2.

Criterion	Description	Value	Detail
0	Temperature drift in EQ	$< 0.05\,^{\circ}C$	for the last 60 min
1	Overpotential drift in CP	< 0.65 mV	for the last 10 min
2	$\tilde{R}_f$ error in circuit fitting in PEIS	$< 50\,\%$	of fitting value
3	Instant Tafel slope from CP or PEIS	70–80 mV dec^{-1}	this range

an equivalent circuit that is comprised of two time constants associated with OER and other to the contact or ionic resistance. The work of Doyle and coworkers[30] shows another circuit with three time constants that fits most of electrodes covered with passive oxides or hydrous oxides. The work of Zaharieva and coworkers[53] also provides a suitable circuit of two time constants to model the phenomenology. The mentioned equivalent circuits are shown in Section S6 Scheme S3. Orazem and Tribollet[54] discuss about the mathematical equivalence between the frequency response of different physical models in circuits displayed in Scheme S3b and Scheme S3c (when diffusion effects are neglectable) and Scheme S3d (when inner oxide layer is neglectable).

Fitting more complicated models was attempted but did not give better results. As modelling the complete phenomenology of OER on CoCat is out of the scope of this work, and the only objective is to obtain a polarization resistance value as accurate as possible, it was preferred to make a cut in the frequency and only fit the points obtained at frequencies below 5 Hz and to study only one time constant, as it could be demonstrated that both do not overlap in the obtained spectra. Hence, the behavior of this portion of the spectra can be correctly represented by a much simpler Randles cell with CPE instead of capacitor achieving a much lower goodness of fit value with 4 degrees of freedom rather than the 6 required in Scheme S3b[52] (neglecting diffusion/Warburg element), or 7 in Scheme S3c[53] and Scheme S3d[30] respectively, when all the phenomena are included. This way also the convergence of the numerical system into a viable solution is considerably simpler, even in absence of a plausible initial solution guess.

The observed trends (and errors) of the resistances obtained from PEIS can be seen for each fitting in Section S6 Figure S5. R_u decreases with increasing overpotential and temperature as expected for oxidation of CoCat and/or FTO and a semiconductor, respectively.

The conditioning at the end of each iteration is responsible of a slight increase on the polarization resistance, R_p, at the first measurements of each iteration. This is consistent with works that describe the capacity of this material to self-heal at potentials lower than the onset of the OER.[55] R_p, has the expected values and changes with increasing OER overpotential with an exponential decay. As it was already mentioned, the charge is predominantly due to OER and not to oxidative changes in Co atoms without producing oxygen as the PEIS was preceded by a CP at the same DC potential. In conclusion, DRT spectra, the low chi square values obtained in the fitting and the highly similitude between the results acquired by both approaches supported that the PEIS approach can provide thermodynamic values for the RDS as well as SSP.

Comparison of used and obtained parameters with literature

In the work of Sprague-Klein et al[56] a similar experimental Tafel Analysis of CoCat at different temperatures between 20 and 60 °C have been reported but with different research purpose. In the works of Ahn and Bard found in the literature,[27,48] they calculate the kinetic constants between Co^{III} and Co^{IV} sites and H_2O: 1.2[48] and 3.2 s^{-1}[27] at $\eta = 410$ mV, respectively. This coverage value was obtained by surface interrogation scanning electrochemical microscopy (SI-SECM). Also, Lee and collaborators[17] have performed very similar calculations but with a LSV at 20 mV s^{-1} instead of SSP.

Now we proceed to compare the values reported in the forementioned works with this one in each parameter investigated (for complete results coming from each dataset refer to Section S9):

(1) Current density (j) range: The range used in this work spans from $10^{-4.25}$ to $10^{-2.25}$ A cm^{-2} (5.5 to 555 μA cm^{-2}) chronopotentiometrically. 0 to 100 μA cm^{-2} used for fitting. Lee and collaborators[17] study $10^{-3.5}$ to 10^{-2} A cm^{-2} (316 μA cm^{-2} to 10 mA cm^{-2}) and Sprague-Klein et al[56] $10^{-3.25}$ to 10^{-3} A cm^{-2} (562 μA cm^{-2} to 1 mA cm^{-2}), both chronoamperometrically.

(2) Temperature (T) range: This work: 25 to 40 °C. Sprague-Klein et al[56] 20 and 60 °C, Lee and collaborators[17] 20 to 70 °C The other groups aim to higher temperatures, but the duration of their experiments is also shorter compared to ours.

(3) Overpotential range (η): This work: 360 to 440 mV at 25 °C and (390 to 410 mV at 25 °C for fitting). Lee and collaborators[17] 420 to 510 mV. Sprague-Klein et al[56] 270 360 mV.

(4) Tafel slope (b): This work: 68 to 78 mV dec^{-1} SSP. 64 to 72 mV dec^{-1} PEIS. Lee and collaborators[17] near 70 mV dec^{-1}. Sprague-Klein et al[56] 61 and 76 mV dec^{-1}. We emphasize the dependence on the current/overpotential window chosen to have a slope value higher or lower. This has also relation with the range of overpotentials chosen in[56] as its boundaries are lower than the boundaries we used or also in.[17]

(5) Exchange current density (j^0): This work: 0.09 to 0.13 nA cm^{-2} from SSP. 0.04 to 0.08 nA cm^{-2} from PEIS. Sprague-Klein et al[56] 20 and 120 nA cm^{-2}. Lee and collaborators[17] $j^0 = 0.19$ nA cm^{-2}. Regarding to the x-axis intercepts of the Tafel plots (j^0) the value depends strongly on the way the conversion to overpotential has been done.

(6) Transfer coefficient (β): This work: 0.81 to 0.84. Lee and collaborators[17] 0.94. Sprague-Klein et al[56] 0.87 to 0.95. Our β is smaller than previously reported. First, $\beta = 0.94$ is related to a Tafel slope of ca 63 mV dec^{-1} at 298 K (Equation 6) whereas our instant Tafel slope range is between 70 and 80 mV dec^{-1} at temperatures between 25 and 40 °C due to Criterion 3 and for this range using the same equation and temperature $\beta = 0.81$ (73 mV dec^{-1}) and 0.84 (70 mV dec^{-1}) for SSP and PEIS respectively.

(7) Density of active sites (Γ_{act}): This work: 50 Co atoms per nm^2 or $5.0 \cdot 10^{15}$ cm^{-2}. Ahn and Bard[27] 11 Co atoms per nm^2 or $1.1 \cdot 10^{15}$ cm^{-2}. Our density of active sites is likely overestimated as not all Co^{IV} may reduce to Co^{II}. Yet, the order of magnitude agrees with the previous study.

(8) Kinetic constant extrapolated to zero overpotential (k^0) at 25 °C: This work: $3.07 \cdot 10^{-8}$ and $5.6 \cdot 10^{-8}$ s^{-1} for SSP and PEIS respectively. Lee and collaborators[17] $2.7 \cdot 10^{-7}$ s^{-1} at $\eta = 0$. Ahn and Bard 3.2 s^{-1}[27] at $\eta = 410$ mV (TOF).

(9) Gibbs Free energy extrapolated to zero overpotential at 25 °C ($\Delta^{\neq}G^0$): This work: 1.21 eV SSP, 1.20 eV PEIS. 1.15 eV. Ahn and Bard[27]

(10) Enthalpy extrapolated to zero overpotential ($\Delta^{\neq}H^0$): This work: 0.72 eV SSP, 0.81 eV PEIS. Lee and collaborators[17] 0.74 eV.

(11) Entropy at 25 °C ($T^{\circ}\Delta^{\neq}S$): This work: −0.48 eV SSP, −0.39 PEIS. Lee and collaborators[17] −0.41 eV (using Gibbs Free energy from Ahn and Bard).

Another aspect worthy mentioning is that the effect that the entropic contribution has to the energetic span of OER catalytic cycle is considerable compared to the total Gibbs free energy part in both sets (35 % using Lee and coworkers' values, 39.6 % and 32.5 % using our two approaches). In our case we used 50 Co atoms per nm^2 as a coverage value (refer to Section S7). In comparison with SI-SECM, we would like to remark the fact of the simplicity of the CV as a method to estimate the reductive charge for transition metal based electrocatalysts where SI-SECM analysis is not available, and the attenuated effect this would have in the precision of the entropy obtained, as in Equations 1 h and 3 h the coverage is inside a logarithm. In summary, our determined values agree mostly with literature and reasons for deviations have been discussed.

Two methods were used herein to obtain key thermodynamic parameters, which gave identical results within a single standard deviation for β, $\Delta^{\neq}$ H, $T^{\circ}\Delta^{\neq}S$ and $\Delta^{\neq}$ G^0. The SPP approach has the simpler analysis as compared to PEIS, which requires fitting to a suitable model. We expect that PEIS becomes superior to SPP for more complex electrocatalytic systems where different processes need to be distinguished and when capacitive contributions to the current are not negligible as compared to the faradaic (oxidative) contribution. Our model electrocatalyst was selected for simplicity so that SPP and PEIS were equally accurate. Yet, the SPP approach resulted in smaller standard deviations and thus better precision as compared to the PEIS approach for our model system, which we attribute to the simpler analysis. Further work on more complex electrocatalyst systems is needed to conclusively evaluate the strengths and weaknesses of the two methods.

Conclusions

In this work we present two ways of determining the thermodynamic values of the RDSI for OER in a model catalyst: The SSP approach and the PEIS approach. The first one uses series of chronopotentiometries at different current and temperature values. The second one uses potentiostatic EIS measurements at different DC potentials and different temperatures. The datasets from both approaches were fitted by modified a tridimensional Eyring-Polanyi equation using biplanar regression. From the slopes of the fits, we obtained the enthalpy of the RDSI and its associated transfer coefficient. Likewise, we determined the entropy of the RDSI from the intercept in these plots, knowing a priori the surface density of active sites, which was herein approximated by integrating the reductive charge from CV. We discussed main sources of error: The most important factor is not reaching SSPC, which implies that the temperature and overpotential (in case of using CP) were invariant in time. The second most important factor was an accurate choice of a region with Tafel behavior. We proposed four criteria for filtering the experimental dataset to mitigate these sources of error.

The enthalpy and entropy values that we obtained for RDSI of CoCat at pH = 7 are consistent with values obtained in the literature. Our protocol can be readily extended to other electrocatalysts and electrocatalytic reactions and we hope that it generates data that can be readily compared to theoretical kinetics studies. The two approaches which were equally accurate but the SPP approach was more precise for a simple electrocatalytic system such as CoCat. We expect that the PEIS approach unfolds its full potential for more complex electrocatalyst systems.

Abbreviation

AC	Altern current
CA	chronoamperometry
CE	counter electrode
CHE	computational hydrogen electrode
CoCat	amorphous cobalt oxide phosphate catalyst
CP	chronopotentiometry
CPE	constant phase element
CV	cyclic voltammetry
DC	direct current
DRC	degree of rate control of a step in the overall reaction rate
DFT	density functional theory
DRT	distribution of relaxation times
EIS	electrochemical impedance spectroscopy
EQ	equilibration step
FTO	fluorine-doped tin oxide
HER	hydrogen evolution reaction
LSV	linear sweep voltammetry
MD	molecular dynamics
NHE	normal hydrogen electrode
OCP	open circuit potential
OER	oxygen evolution reaction
PDS	potential determining step
PEIS	potentiostatic electrochemical impedance spectroscopy
RDSI	rate determining state and intermediate
RE	reference electrode

RHE	reversible hydrogen electrode
S	state
SI	supporting information
SI-SECM	surface interrogation scanning electrochemical microscopy
SSP	steady state polarization approach
SSPC	steady state polarization condition
TOF	Turnover frequency
TS	transition state
TST	transition state theory
WE	working electrode
WSR	water splitting reaction

Acknowledgements

This project has received funding from the European Research Council (ERC) under the European Union's Horizon 2020 research and innovation program under grant agreement No 804092. Open Access funding enabled and organized by Projekt DEAL.

Conflict of Interests

The author declare no conflict of interest.

Data Availability Statement

The data that support the findings of this study are openly available in Zenodo at https://doi.org/10.5281/zenodo.10222127, reference number 10222127.[49]

Keywords: OER rate-limiting state · OER rate-determining state enthalpy · OER mechanism · Eyring-Polanyi · cobalt oxides

[1] Accelerating Hydrogen Deployment in the G7: Recommendations for the Hydrogen Action Pact, *International Renewable Energy Agency*, Abu Dhabi, **2022**.
[2] Z. Yu, Y. Duan, X. Feng, X. Yu, M. Gao, S. Yu, *Adv. Mater.* **2021**, *33*, 2007100.
[3] L. An, C. Wei, M. Lu, H. Liu, Y. Chen, G. G. Scherer, A. C. Fisher, P. Xi, Z. J. Xu, C. Yan, *Adv. Mater.* **2021**, *33*, 2006328.
[4] B. Guo, Y. Ding, H. Huo, X. Wen, X. Ren, P. Xu, S. Li, *Nano-Micro Lett.* **2023**, *15*, 57.
[5] S. Wang, T. Shen, C. Yang, G. Luo, D. Wang, *ACS Catal.* **2023**, *13*, 8670–8691.
[6] M. Risch, *Curr. Opin. Electrochem.* **2023**, *38*, 101247.
[7] N.-T. Suen, S.-F. Hung, Q. Quan, N. Zhang, Y.-J. Xu, H. M. Chen, *Chem. Soc. Rev.* **2017**, *46*, 337–365.
[8] P. Sabatier, *Ber. Dtsch. Chem. Ges.* **1911**, *44*, 1984–2001.
[9] I. C. Man, H. Su, F. Calle-Vallejo, H. A. Hansen, J. I. Martínez, N. G. Inoglu, J. Kitchin, T. F. Jaramillo, J. K. Nørskov, J. Rossmeisl, *ChemCatChem* **2011**, *3*, 1159–1165.
[10] K. S. Exner, *ACS Catal.* **2020**, *10*, 12607–12617.
[11] W. T. Hong, M. Risch, K. A. Stoerzinger, A. Grimaud, J. Suntivich, Y. Shao-Horn, *Energy Environ. Sci.* **2015**, *8*, 1404–1427.
[12] M. G. Evans, M. Polanyi, *Trans. Faraday Soc.* **1935**, *31*, 875.
[13] C. Amatore, A. Jutand, *J. Organomet. Chem.* **1999**, *576*, 254–278.
[14] S. Kozuch, S. Shaik, *Acc. Chem. Res.* **2011**, *44*, 101–110.
[15] K. S. Exner, H. Over, *ACS Catal.* **2019**, *9*, 6755–6765.
[16] R. Parsons, *Trans. Faraday Soc.* **1951**, *47*, 1332.
[17] K.-G. Lee, M. Balamurugan, S. Park, H. Ha, K. Jin, H. Seo, K. T. Nam, *ACS Energy Lett.* **2019**, *4*, 1918–1929.
[18] C. T. Campbell, *Top. Catal.* **1994**, *1*, 353–366.
[19] C. T. Campbell, *ACS Catal.* **2017**, *7*, 2770–2779.
[20] K. S. Exner, *J. Energy Chem.* **2023**, *83*, 247–254.
[21] H. Pham, M. Cheng, H. Frei, L. Wang, *ACS Catal.* **2016**, *6*, 5610–5617.
[22] J. Mefford, Z. Zhao, M. Bajdich, W. Chueh, *Energy Environ. Sci.* **2020**, *13*, 622–634.
[23] L. Wang, T. Van Voorhis, *J. Phys. Chem. Lett.* **2011**, *2*, 2200–2204.
[24] C. Davidson, G. Kissel, S. Srinivasan, *J. Electroanal. Chem.* **1982**, *132*, 129–135.
[25] B. Zhang, X. Zheng, O. Voznyy, R. Comin, M. Bajdich, M. García-Melchor, L. Han, J. Xu, M. Liu, L. Zheng, F. P. García de Arquer, C. T. Dinh, F. Fan, M. Yuan, E. Yassitepe, N. Chen, T. Regier, P. Liu, Y. Li, P. De Luna, A. Janmohamed, H. L. Xin, H. Yang, A. Vojvodic, E. H. Sargent, *Science* **2016**, *352*, 333–337.
[26] X. Zheng, B. Zhang, P. De Luna, Y. Liang, R. Comin, O. Voznyy, L. Han, F. P. García de Arquer, M. Liu, C. T. Dinh, T. Regier, J. J. Dynes, S. He, H. L. Xin, H. Peng, D. Prendergast, X. Du, E. H. Sargent, *Nat. Chem.* **2018**, *10*, 149–154.
[27] H. Ahn, A. Bard, *J. Am. Chem. Soc.* **2015**, *137*, 612–615.
[28] F. Song, L. Bai, A. Moysiadou, S. Lee, C. Hu, L. Liardet, X. Hu, *J. Am. Chem. Soc.* **2018**, *140*, 7748–7759.
[29] H. Seo, K. H. Cho, H. Ha, S. Park, J. S. Hong, K. Jin, K. T. Nam, *J. Korean Ceram. Soc.* **2017**, *54*, 1–8.
[30] R. Doyle, I. Godwin, M. Brandon, M. Lyons, *Phys. Chem. Chem. Phys.* **2013**, *15*, 13737.
[31] M. Kanan, D. Nocera, *Science* **2008**, *321*, 1072–1075.
[32] Y. Surendranath, M. Kanan, D. Nocera, *J. Am. Chem. Soc.* **2010**, *132*, 16501–16509.
[33] Y. Surendranath, M. Dincaˇ, D. G. Nocera, *J. Am. Chem. Soc.* **2009**, *131*, 2615–2620.
[34] M. Risch, K. Klingan, I. Zaharieva, H. Dau, in *Molecular Water Oxidation Catalysis*, John Wiley & Sons, Ltd, **2014**, pp. 163–185.
[35] M. R. Mohammadi, S. Loos, P. Chernev, C. Pasquini, I. Zaharieva, D. González-Flores, P. Kubella, K. Klingan, R. D. L. Smith, H. Dau, *ACS Catal.* **2020**, *10*, 7990–7999.
[36] P. Zhang, Y. Dong, Y. Kou, Z. Yang, Y. Li, X. Sun, *Catal. Lett.* **2015**, *145*, 1169–1176.
[37] H. Kim, J. Park, I. Park, K. Jin, S. E. Jerng, S. H. Kim, K. T. Nam, K. Kang, *Nat. Commun.* **2015**, *6*, 8253.
[38] A. Grimaud, O. Diaz-Morales, B. Han, W. T. Hong, Y.-L. Lee, L. Giordano, K. A. Stoerzinger, M. T. M. Koper, Y. Shao-Horn, *Nature Chem* **2017**, *9*, 457–465.
[39] M. Bajdich, M. García-Mota, A. Vojvodic, J. K. Nørskov, A. T. Bell, *J. Am. Chem. Soc.* **2013**, *135*, 13521–13530.
[40] A. H. Motagamwala, M. R. Ball, J. A. Dumesic, *Annu. Rev. Chem. Biomol. Eng.* **2018**, *9*, 413–450.
[41] A. H. Motagamwala, J. A. Dumesic, *Chem. Rev.* **2021**, *121*, 1049–1076.
[42] G. Mattioli, P. Giannozzi, A. Amore Bonapasta, L. Guidoni, *J. Am. Chem. Soc.* **2013**, *135*, 15353–15363.
[43] K. Exner, H. Over, *Acc. Chem. Res.* **2017**, *50*, 1240–1247.
[44] R. Guidelli, R. G. Compton, J. M. Feliu, E. Gileadi, J. Lipkowski, W. Schmickler, S. Trasatti, *Pure Appl. Chem.* **2014**, *86*, 245–258.
[45] S. Fletcher, *J. Solid State Electrochem.* **2009**, *13*, 537–549.
[46] S. Anantharaj, S. Noda, M. Driess, P. Menezes, *ACS Energy Lett.* **2021**, 1607–1611.
[47] A. T. Marshall, L. Vaisson-Béthune, *Electrochem. Commun.* **2015**, *61*, 23–26.
[48] H. S. Ahn, A. J. Bard, *Anal. Chem.* **2015**, *87*, 12276–12280.
[49] J. Morales-Santelices, **2024**, DOI 10.5281/zenodo.10222127.
[50] J. Villalobos, R. Golnak, L. Xi, G. Schuck, M. Risch, *J. Phys. Energy* **2020**, *2*, 034009.
[51] I. Katsounaros, J. C. Meier, S. O. Klemm, A. A. Topalov, P. U. Biedermann, M. Auinger, K. J. J. Mayrhofer, *Electrochem. Commun.* **2011**, *13*, 634–637.
[52] K. E. Neerugatti, S. Adhikari, D.-H. Kim, J. Heo, *Appl. Catal. B* **2021**, *292*, 120192.
[53] I. Zaharieva, D. González-Flores, B. Asfari, C. Pasquini, M. R. Mohammadi, K. Klingan, I. Zizak, S. Loos, P. Chernev, H. Dau, *Energy Environ. Sci.* **2016**, *9*, 2433–2443.
[54] M. E. Orazem, B. Tribollet, in *Electrochemical Impedance Spectroscopy*, John Wiley & Sons, Ltd, **2008**, pp. 61–72.
[55] C. Costentin, D. G. Nocera, *Proc. Natl. Acad. Sci. USA* **2017**, *114*, 13380–13384.

[56] E. A. Sprague-Klein, X. He, M. W. Mara, B. J. Reinhart, S. Lee, L. M. Utschig, K. L. Mulfort, L. X. Chen, D. M. Tiede, *ACS Energy Lett.* **2022**, *7*, 3129–3138.
[57] K. Exner, I. Sohrabnejad-Eskan, H. Over, *ACS Catal.* **2018**, *8*, 1864–1879.
[58] J. K. Nørskov, J. Rossmeisl, A. Logadottir, L. Lindqvist, J. R. Kitchin, T. Bligaard, H. Jónsson, *J. Phys. Chem. B* **2004**, *108*, 17886–17892.
[59] G. Peckham, I. McNaught, *J. Chem. Educ.* **2011**, *88*, 782–783.
[60] S. G. Bratsch, *J. Phys. Chem. Ref. Data* **1989**, *18*, 1–21.
[61] K. Klingan, F. Ringleb, I. Zaharieva, J. Heidkamp, P. Chernev, D. Gonzalez-Flores, M. Risch, A. Fischer, H. Dau, *ChemSusChem* **2014**, *7*, 1301–1310.
[62] D. Antipin, M. Risch, *Electrochem. Sci. Adv.* **2022**.
[63] A. DeBethune, T. Licht, N. Swendeman, *J. Electrochem. Soc.* **1959**, *106*, 616.
[64] T. J. Smith, K. J. Stevenson, in *Handbook of Electrochemistry* (Ed.: C. G. Zoski), Elsevier, Amsterdam, **2007**, pp. 73–110.
[65] A. J. Bard, L. R. Faulkner, *Electrochemical Methods: Fundamentals and Applications*, *2nd Edition*, John Wiley & Sons, Incorporated, **2000**.
[66] W. Xing, M. Yin, Q. Lv, Y. Hu, C. Liu, J. Zhang, in *Rotating Electrode Methods and Oxygen Reduction Electrocatalysts* (Eds.: W. Xing, G. Yin, J. Zhang), Elsevier, Amsterdam, **2014**, pp. 1–31.

Manuscript received: November 30, 2023
Revised manuscript received: January 31, 2024
Accepted manuscript online: February 5, 2024
Version of record online: February 21, 2024